Landscape Recognition Algorithm for Polarized Detector based on Optimal Projection

Xiao-rong TONG

Abstract—In this paper, a novel landscape recognition algorithm based on the optimal projection is proposed to meet the landscape measurement requirements of a detector. The proposed algorithm is applied to the airborne radar platform, proving a necessary recognition ability. The characteristic values of the target scattering matrix eigenvalues are defined, which has no direct relation to the power and angle of a detection signal and is only related to the topographic features of a landscape in the detection range. Besides, a series of standard scatter rotation invariant matrices with uncertain parameters are constructed based on the Krogager's idea of decomposing the target scattering matrices. The geomorphological polarization scattering matrix of a detection range is projected onto the standard scatter projects, and relevant weight values are calculated to judge the landscape attributes so as to achieve the goal of landscape recognition. Effective landscape recognition can further enhance the autonomous ability of ammunition and overcome the effects of a new diversified operational environment.

Index Terms—polarized signal, optimal projection, airborne radar platform, landscape recognition, rotation invariant matrix

I. INTRODUCTION

BY employing the vector characteristics of the electromagnetic wave, a polarized detector obtains the polarized scattering response characteristics of a target [1], [2], which are extremely sensitive to the target's dielectric constant, geometric shape, and spatial orientation. Therefore, by using a polarized detector, the acquisition capability of the target's physical properties can be enhanced [3]. The polarization target recognition method has been applied and validated in different domains, and favorable recognition performances have been achieved. Wang F Y et al. proposed a novel type of polarized invariant features for radar target recognition, achieving the mean recognition accuracy of over 90% and 80% [4]. However, this method needs to train the polarized invariant features and has a long response time. Shao X H et al. proposed a complex-weighing-based target polarization recognition method for unknown and time-varying clutter environment. Moreover, they extracted the polarization characteristics of the target echoes and achieved higher recognition accuracy than the traditional recognition algorithm such as forward-looking imaging, HRRP (High Resolution Range Profile) and so on [5]. Beauchamp et al. used the dual-polarization radar scattering characteristics for recognition, analyzed the target's motion and structural characteristics in detail, and successfully recognized wind turbines on the ground. However, by using this method, the detect end cannot acquire the complete target information of unknown and non-cooperative targets, suggesting that this method is unfavorable for target recognition on a battlefield [6].

Due to the limited platform space, complex motion states, and short flight time, some of the mature polarization target recognition techniques and algorithms are not applicable to a low-attitude flight platform. At present, the research on the detection by a low-altitude flight platform mainly focuses on detector design and detecting strategy. Xu R et al. studied the design of a missile-borne real-time radar signal processing system profoundly and proposed a standardized module and expandable system design scheme, which can address the problem of real-time receiving and processing of a missile-borne radar signal [7]. Chen Y et al. proposed a SAR imaging algorithm based on the fractional Fourier transform [8]. Because an echo signal undergoes the independent local optimal processing during the imaging process, this method is applicable to a non-linear flight path of a missile platform [8]. Song L Z et al. designed a linear frequency modulation (LFM) or a phase-coded pulse compression signal in the transmitting pulse [9], and this guidance radar system possesses favorable frequency-shift jamming and delay-interference resistance abilities. Motivated by the above research results, this paper aims to establish a landscape recognition algorithm for a polarized detector on a low-attitude flight platform, which can endow the platform with the capability of self-recognition of the ground objects, and thus acquire the landscape recognition capability.

Xiao-rong Tong is with the College of Computer, Weinan Normal University, Weinan, 714099 China (phone: 13309130852; e-mail: wnsyjsjkxx@163.com).

II. LANDSCAPE RECOGNITION ALGORITHM BASED ON POLARIZED OPTIMAL PROJECTION

According to Krogager's research results, the polarization scattering matrix of any object can be decomposed into three components, namely, spheroid, dihedral angle, and spirochete [10]. Thus, different targets can be recognized based on a difference in their compositions. As shown in Fig. 1, a low-attitude flight platform can detect complex terrains including mountains and hills.
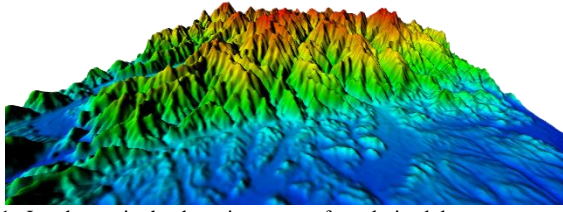
Fig. 1. Landscape in the detection range of a polarized detector.

As shown in Fig. 1, regarding the geomorphic features, different landforms differ slightly after the decomposition into a spheroid, dihedral angle, and spirochete. In this study, standard component bodies are improved to increase the difference and contribute to the recognition of the geomorphic features.

A. Rotational Invariant Parameters of Scattering Matrix

The polarization characteristic quantities irrelevant to the position and observation angle should be constructed during the target recognition by a polarized detector. For a mono-station radar, when the reciprocal theory is satisfied, the target scattering matrix represents an axial-symmetry matrix, and can be expressed as:

$$S = \begin{bmatrix} S_{hh} & S_{hv} \\ S_{vh} & S_{vv} \end{bmatrix}, \qquad (1)$$

where $S_{hv} = S_{vh}$, the subscript 'ij' relates to the signal emitted in the jth polarization mode and received by the ith polarization model, h denotes the horizontal polarization, and v denotes the vertical polarization. As the incident angle changes, the target scattering matrix can be expressed as:

$$S(\theta) = J(\theta) \cdot S \cdot J(-\theta), \qquad (2)$$

where $J(\theta)$ denotes the rotational function and can be expressed as:

$$J(\theta) = \begin{bmatrix} \cos\theta & -\sin\theta \\ \sin\theta & \cos\theta \end{bmatrix}. \qquad (3)$$

Since it can be easily proved that $J(-\theta) = J^{-1}(\theta)$, the following expression can be derived:

$$[J(\theta) \cdot P]^{-1} \cdot S \cdot [J(\theta) \cdot P] = \begin{bmatrix} \lambda_1 & \omega \\ 0 & \lambda_2 \end{bmatrix}. \qquad (4)$$

According to (4), when the scattering matrix rotates by a certain angle θ, the acquired new scattering matrix and original matrix have an identical upper triangular matrix. Based on the related matrix theories, the value of ω can be only 0 or 1. Namely, when $\lambda_1 = \lambda_2$, then $\omega = 1$; otherwise, when $\lambda_1 \neq \lambda_2$, then $\omega = 0$.

B. Optimal Projection of Scattering Matrix

To measure the similarity degree between the geomorphic features in the detection range and the base, an optimal projection distance (OPD) of the scattering matrix is introduced. The measure vector can be defined as:

$$k = [\lambda_1 \quad \lambda_2 \quad x]^{T}, \qquad (5)$$

where $|\lambda_1| \geq |\lambda_2|$, and the subscript ^{T} represents the transposition process. Then, x can be expressed as:

$$x = \omega \cdot \sqrt{|S_{hh}|^2 + 2|S_{hv}|^2 + |S_{vv}|^2}. \qquad (6)$$

According to the theory presented in Section 2.1, it can be easily derived that the measure vector k is a rotational invariant vector and can be used for similarity analysis between the scattering matrices. Assume that the scattering matrices of echo and basement are denoted as S_1 and S_2, respectively, and that their measure vectors are k_1 and k_2, respectively. Then, the OPD of S_1 to S_2 can be expressed as:

$$c_{OPD}(S_1 \quad S_2) = \max\left[\frac{\left|(k_1)^{T} \cdot k_2\right|^2}{\|k_1\|_2^2 \cdot \|k_2\|_2^2} \right]. \qquad (7)$$

According to Eq. (7), $c_{OPD}(S_1 \quad S_2) \in [0,1]$, and when and only when $S_1 = P \cdot S_1 \cdot P^{-1}$, then $c_{OPD}(S_1 \quad S_2) = 1$. By solving the optimal polarization projection problem, the components of a geomorphic environment within the detection range can be acquired.

C. Analysis of Various Basements in New Projection Base

A new projection base composed of a rectangular pyramid, a circular truncated cone, and a sphere is established. Assume that φ and ψ denote the elevation angle and azimuth angle of a detection beam, respectively.

Basement 1 is defined as a rectangular pyramid (RP) wherein various bottom edges have the same heights, i.e., the angle between the side surface and each bottom is 45°. Within the detection range ($0° < \varphi < 60°$ and $-60° < \psi < 60°$), the rotational invariant parameter matrices of different bases are solved, and the far-field settings of the RP are displayed in Fig. 2.

(a) Horizontal polarization input settings of the RP
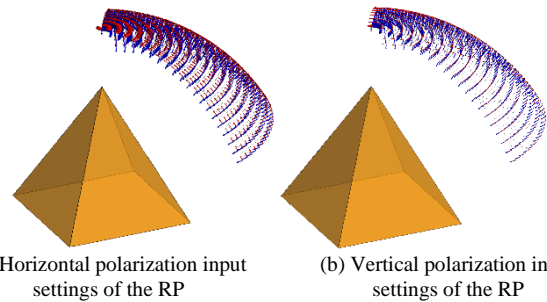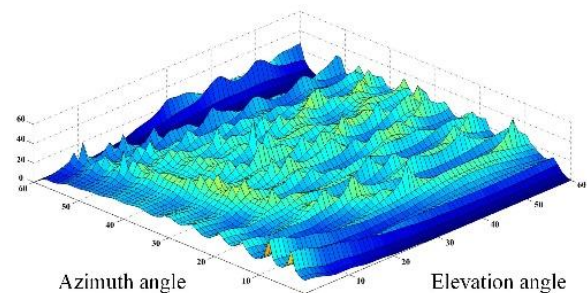(b) Vertical polarization input settings of the RP

Fig. 2. Horizontal and vertical polarization input settings of the basement 1 within the detection range.

According to the above inputs, the scattering matrix of the basement 1 at every angle is expressed as:

$$S_{RP} = S_{RP\_0} \cdot \Theta_1(\psi) \cdot \Theta_2(\varphi), \qquad (8)$$

where S_{RP} denotes the scattering matrix of the basement 1 at any beam incident angle, S_{RP_0} denotes the scattering matrix of the basement 1 at zero positions ($\varphi = 0°$ and $\psi = 0°$), and Θ_i denotes the rotational function at different angles within the detection angle so that S_{RP} can traverse the range at any angle. The values of various elements of the scattering matrix are presented in Fig. 3.

(a) Horizontal transmission and horizontal receiving

(b) Horizontal transmission and vertical receiving
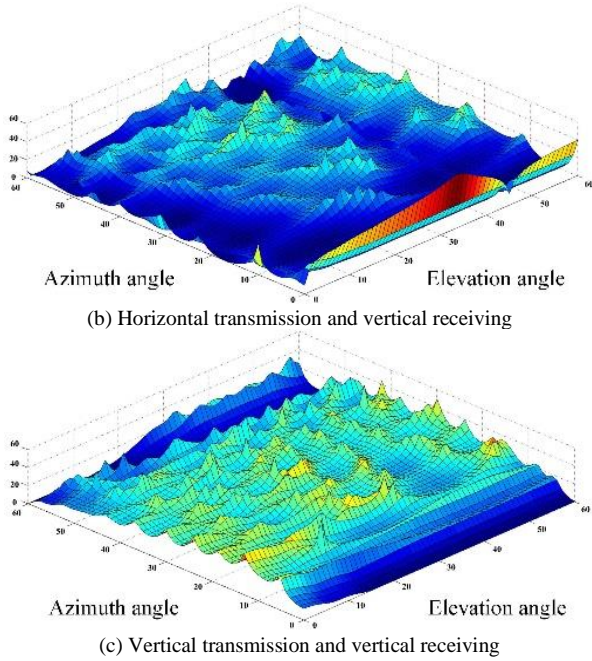

(c) Vertical transmission and vertical receiving

Fig. 3. The scattering matrix elements under different azimuth polarization conditions.

By solving the basement polarization scattering matrix at different angles, the measure vector under different conditions can be obtained and then used to determine the distances between the geomorphic features of the target region and those of the basement 1 so as to judge the similarity.

The basement 2 is defined as a truncated cone (TC), in which the angle between the bottom and the side surfaces is 45°, i.e., the ratio of the bottom radius to the height is $1/\sqrt{3}$, and the radius of the upper disk is half of that of the lower disk. Within the detection range ($0° < \varphi < 60°$), the rotational invariant parameter matrices of different bases were solved, as the far field setting displayed in Fig. 4.

(a) Horizontal polarization input settings of the TC

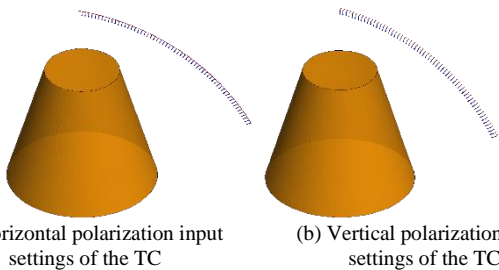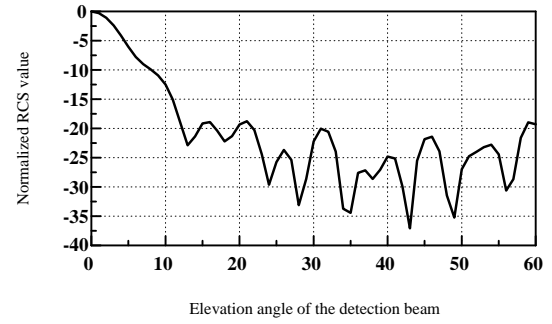(b) Vertical polarization input settings of the TC

Fig. 4. Horizontal and vertical polarization input settings of the basement 2 within the detection range.
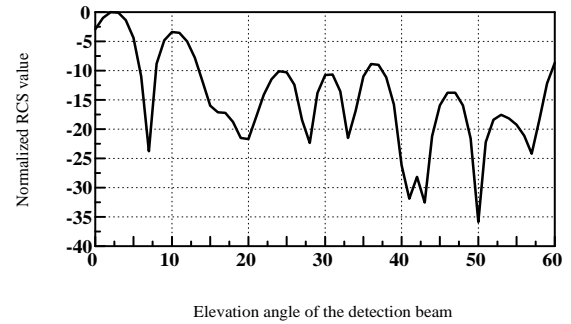
According to the above inputs, the scattering matrix of the basement 2 at each angle is expressed as:

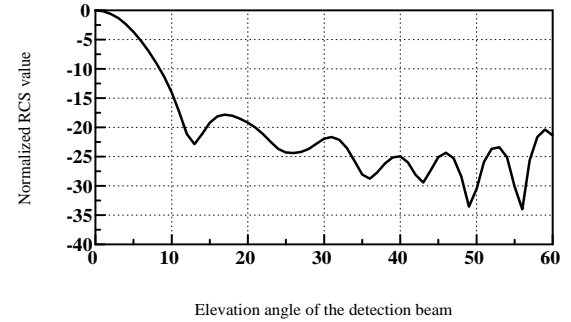$$S_{TC} = S_{TC\_0} \cdot \Theta_1(\varphi), \qquad (9)$$

where S_{TC} denotes the scattering matrix of the basement 2 at any beam incident angle, S_{TC_0} denotes the scattering matrix of the basement 2 at zero positions ($\varphi = 0°$), and Θ_i denotes the rotational function at different angles within the detection angle so that S_{TC} can traverse the range at any angle. The values of various elements of the scattering matrix are presented in Fig. 5.

(a) Normalized RCS value for the horizontal-horizontal polarization pattern within the detection range

(b) Normalized RCS value for the horizontal-vertical polarization pattern within the detection range

(c) Normalized RCS value for the vertical-vertical polarization pattern within the detection range

Fig. 5. Normalized RCS value under different polarization conditions.

Similarly, the measure vectors of the basement 2 under different conditions can be obtained by solving the RCS of the basement at different beam elevation angles; accordingly, the distances between the geomorphic features of the target region and that of the basement 2 can be calculated by the judgement of similarity.

Basement 3 is defined as a spheroid.

According to the analysis of a spheroid scattering matrix described in [11], a spheroid scattering matrix can be described as:

$$S_s = \begin{bmatrix} 1 & 0 \\ 0 & 1 \end{bmatrix}. \qquad (10)$$

Then, the measure vector of a spheroid can be expressed as:

$$k_s = \begin{bmatrix} 1 & 1 & 0 \end{bmatrix}^{\mathrm{T}}. \qquad (11)$$

Therefore, both scattering and measure matrices of a spheroid at different detecting angles can be determined.

D. Judgment of Terrain Undulation Degree

According to the landscape recognition and classification methods proposed in [12], the terrain undulation degree can be described by a difference between the maximum and minimum elevations in the region, which is also denoted as

the undulation factor of a detection region. Based on different basement characteristics, the undulation degrees of terrains are set. The undulation degree of basement 3 is a constant, and it is equal to 1, which can be expressed as:

$$T_{ud\_S} = 1 . \tag{12}$$

Assuming T_{ud_RP} and T_{ud_TC} denote the undulation degrees of the basement 1 and basement 2, respectively, the following expression can be written:

$$T_{ud\_i} = (-1)^n \cdot \frac{dis(x_{opt} \quad x_{\Theta})}{dis_{max}} , \tag{13}$$

where $dis(\ )$ denotes the distance function, which is given by:

$$dis(x \quad y) = \sqrt{\sum_{1}^{n}(x_n - y_n)^2} , \tag{14}$$

where x_{opt} denotes the angle coordinate corresponding to the optimal projection, x_{opt} denotes the angle coordinate at the detection boundary, and dis_{max} denotes the maximum distance at the detection boundary [13].

The amplitudes under different polarization modes characterize the profile (shape) characteristics of terrains in the region, and the geomorphic characteristics within certain detection range can be determined only by using combinations of different amplitudes (which is similar to

coordinates). In this study, the optimal projection coordinates during the data processing are expressed as:

$$env_{dec} = [a_{HH} \quad a_{HV} \quad a_{VV}] . \tag{15}$$

Since different basements differ in undulation, when $i = RP$, then $n = 0$, and when $i = TC$, then $n = 1$. The terrain undulation degree within the detection range can be defined as [14]:

$$T_{landscape} = env_{dec} \cdot [T_{ud\_RP}, T_{ud\_TC}, T_{ud\_S}]^T . \tag{16}$$

Consequently, a greater value of $T_{landscape}$ implies a greater region undulation degree. The undulation degree is mainly caused by the existence of multiple peaks in a terrain (similar to basement 1).

III. EXPERIMENTAL VALIDATION

The surface data (22°54, N~232°08, N and 1052°29' E~1052°49 E) of the China-Vietnam border was extracted to validate the feasibility and superiority of the proposed landscape recognition algorithm. This region, with the highest altitude of 1682 m, mainly includes hills and has no large-scale flat areas. Before performing the experiments using the proposed algorithm, the ground clutter of three different landscape types was detected by the FMCW hand radar. The obtained test results of bare, grassland and grove landscapes are given in Table 1.

TABLE 1(A)
FITTING TEST RESULTS OF BARE LAND CLUTTER

Pitching angle (°)	Weibull distribution			Rice distribution		Log-normal distribution			Optimal distribution
	$\hat{p}$	$\hat{q}$	K_{wbl}	$\hat{a}$	K_{ric}	$\hat{X}_m$	$\hat{\sigma}$	K_{lgn}	
20	1.8720	2.6201	0.0659	0.1050	0.4505	0.6550	0.8697	0.2692	Weibull
30	1.8568	2.6992	0.0714	0.1370	0.4615	0.6822	0.8602	0.2802	Weibull
40	1.8514	2.8008	0.0714	0.1489	0.5110	0.7182	0.8569	0.2637	Weibull
50	1.8642	2.8855	0.0604	0.1303	0.4945	0.7502	0.8648	0.2802	Weibull
60	1.8622	2.9822	0.0659	0.1546	0.5110	0.7828	0.8636	0.2527	Weibull

TABLE 1(B)
FITTING TEST RESULTS OF GRASSLAND CLUTTER

Pitching angle (°)	Weibull distribution			Rice distribution		Log-normal distribution			Optimal distribution
	$\hat{p}$	$\hat{q}$	K_{wbl}	$\hat{a}$	K_{ric}	$\hat{X}_m$	$\hat{\sigma}$	K_{lgn}	
20	1.6171	3.5234	0.0824	0.1783	0.6264	0.9026	0.6808	0.3571	Weibull
30	1.6269	3.3254	0.0714	0.1625	0.6099	0.8469	0.6896	0.3516	Weibull
40	1.5937	3.1529	0.0815	0.1400	0.6196	0.7863	0.6591	0.3967	Weibull
50	1.5983	3.0581	0.0769	0.1377	0.5679	0.7568	0.6635	0.3846	Weibull
60	1.6105	2.8623	0.0860	0.1006	0.5753	0.6934	0.6749	0.3978	Weibull

TABLE 1(C)
FITTING TEST RESULTS OF GROVE CLUTTER

Pitching angle (°)	Weibull distribution			Rice distribution		Log-normal distribution			Optimal distribution
	$\hat{p}$	$\hat{q}$	K_{wbl}	$\hat{a}$	K_{ric}	$\hat{X}_m$	$\hat{\sigma}$	K_{lgn}	
20	1.5950	1.8608	0.0500	0.5273	0.0510	0.2592	0.9502	0.4337	Rice
30	1.5928	1.8996	0.1449	0.6293	0.0867	0.2794	0.9480	0.4439	Rice
40	1.6072	2.0923	0.0959	0.7859	0.0714	0.3793	0.9622	0.3929	Rice
50	1.6896	2.1080	0.1010	0.9628	0.0765	0.4042	1.0372	0.3418	Rice
60	1.6916	2.2217	0.0908	1.1156	0.0612	0.4572	1.0389	0.3163	Rice

The optimal distribution of different clutter data which is provided in Table 1 was used to realize the actual clutter environment in different experiments, so that, the confidence level of each verification experiment of the proposed

algorithm could be improved. The terrain coordinates within the beam detection range at different detection pitch angles are presented in Fig. 6.
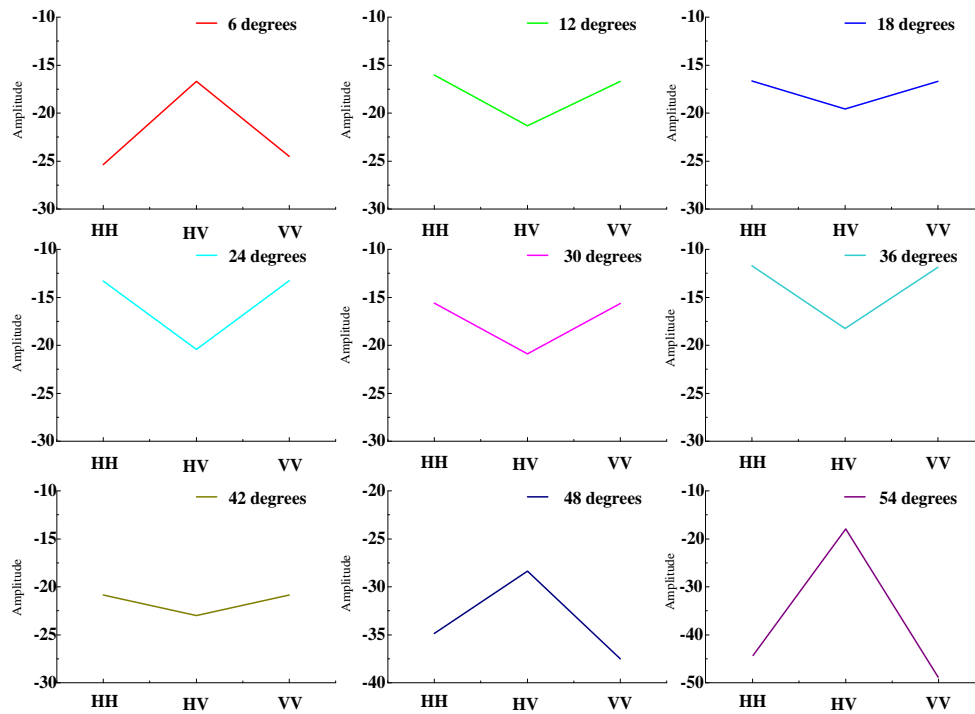
Fig. 6. Terrain coordinates at different detection pitch angles.

Using the obtained coordinates, the measure vector of the target region was determined by using (5) and (6), and the optimal projections of the target region at different angles for different basements were calculated by (7); the obtained results are listed in Table 2. The optimal projection coordinates can reflect the region components, which can also be regarded as the weights of different basements.

TABLE 2
THE RESULTS OF THE MEASUREMENT VECTOR, OPTIMAL PROJECTION, AND UNDULATION DEGREE WITHIN THE TARGET RANGE AT DIFFERENT ANGLES

Pitch angle	Terrain coordinates	Measure vector	Optimal projection onto different basements	Undulation degree
6°	(-25.368, -16.704, -24.503)	$[-41.645, -8.226, 0]^T$	(0.916, 0.469, 0.481)	9.938
12°	(-16.025, -21.321, -16.691)	$[-37.682, 4.965, 0]^T$	(0.826, 0.357, 0.492)	9.044
18°	(-16.658, -19.579, -16.700)	$[-36.258, 2.901, 0]^T$	(0.854, 0.379, 0.497)	9.310
24°	(-13.308, -20.431, -13.256)	$[-33.713, 7.149, 0]^T$	(0.882, 0.321, 0.479)	8.548
30°	(-15.604, -20.887, -15.649)	$[-36.514, 5.261, 0]^T$	(0.822, 0.352, 0.490)	8.966
36°	(-11.728, -18.232, -11.885)	$[-30.039, 6.426, 0]^T$	(0.781, 0.320, 0478)	8.532
42°	(-20.875, -22.996, -20.856)	$[-43.862, 2.130, 0]^T$	(0.868, 0.392, 0.499)	9.444
48°	(-34.879, -28.379, -37.517)	$[-64.608, -7.789, 0]^T$	(0.912, 0.450, 0.493)	9.896
54°	(-44.284, -17.930, -48.794)	$[-64.640, -28.467, 0]^T$	(0.868, 0.494, 0.419)	8.751

As listed in Table 2, a large number of components in this region were similar to basement 1, which also exhibited great undulation. The undulation of this region was quantitatively characterized by the landscape recognition algorithm. Three different terrain types, namely flat and peak, were selected to be recognized quantitatively, so as to reflect the superiority of the proposed algorithm in terrain recognition. Finally, the optimal projections of flat and peak terrains were calculated, and they are listed in Table 3.

TABLE 3
OPTIMAL PROJECTION AND UNDULATION DEGREE OF THE FLAT TERRAIN
AND PEAK TERRAIN AT DIFFERENT PITCH ANGLES

(A) FLAT TERRAIN

Pitch angle	Optimal projection	Undulation degree
6°	(0.084, 0.492, 0.390)	1.326
12°	(0.085, 0.494, 0.405)	1.233
18°	(0.087, 0.494, 0.417)	1.257
24°	(0.090, 0.486, 0.458)	1.398
30°	(0.089, 0.491, 0.445)	1.373
36°	(0.087, 0.494, 0.421)	1.265
42°	(0.088, 0.493, 0.432)	1.411
48°	(0.086, 0.494, 0.415)	1.253
54°	(0.084, 0.493, 0.396)	1.212

(B) PEAK TERRAIN

Pitch angle	Optimal projection	Undulation degree
6°	(0.654, 0.755, 0.245)	7.234
12°	(0.765, 0.732, 0.348)	8.012
18°	(0.799, 0.810, 0.357)	8.320
24°	(0.802, 0.832, 0.249)	8.978
30°	(0.869, 0.812, 0.045)	7.922
36°	(0.900, 0.860, 0.320)	8.265
42°	(0.912, 0.902, 0.144)	9.491
48°	(0.854, 0.820, 0.210)	9.235
54°	(0.897, 0.904, 0.179)	8.902

According to the results in Table 3, different terrains differed greatly in the undulation degree, i.e., the terrain types during the flight can be distinguished through undulation

degree. The proposed algorithm has been used in actual dual polarization radar system, and a series of landscape recognition experiments to prove the superiority of proposed recognition algorithm. Fig. 7 shows the equipment of radar system:

Fig. 7 Dual polarization radar system and measurement equipment

The Pseudo Random Code Continuous Wave (PRC-CW) radar used in the experiment is a type of individual soldier detection radar. The radar is small in size, portable, low in power consumption, high in resolution, strong in anti-interference ability, and has a continuous working time of more than 8 hours under battery power supply. It is suitable for landscape recognition experiments with a certain height of terrain and tripod in the field. We divide the detection area into 101*101 planes, and the recognition results of each points in the detection area are shown in fig. 8 which is the comparison between proposed algorithm and conventional recognition algorithm in different SNRs.
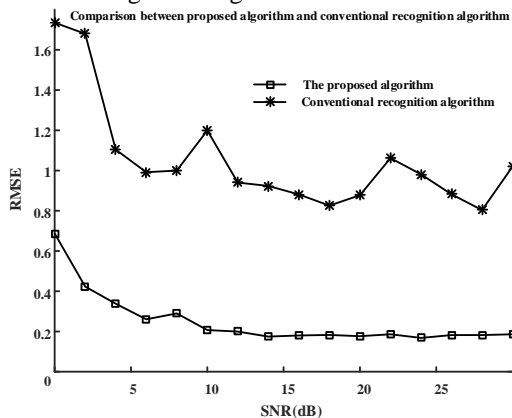

Fig. 8 Recognition RMSE comparison between proposed algorithm and conventional recognition algorithm in different SNRs

In different SNRs conditions, the RMSE results of proposed algorithm are always lower than conventional recognition algorithm. At the first 3 SNR conditions, because of the low signal-to-noise ratio, the recognition error is larger than other SNR conditions. Fig. 9 shows the interface of different number of bit sequence.
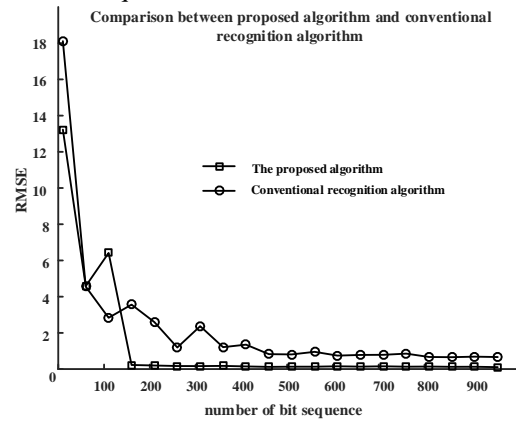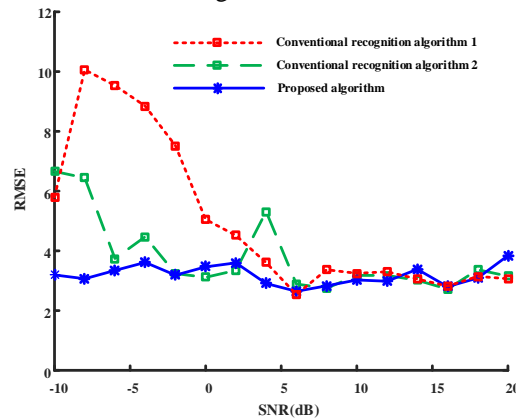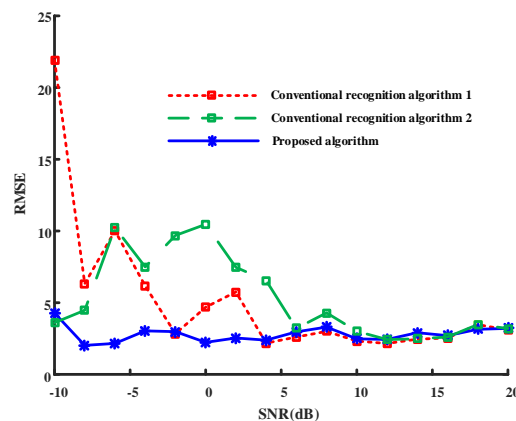

Fig. 9 Comparison results between proposed algorithm and conventional recognition algorithm in different number of bit sequence
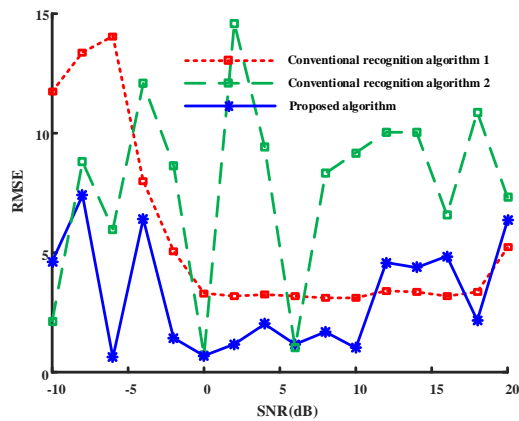
The above simulation results prove the superiority of proposed recognition algorithm, and the whole response of proposed algorithm can meet the requirements the real-time property compare the conventional landscape recognition algorithm. With the increase of signal-to-noise ratio and sampling points, the proposed algorithm has lower recognition error than the traditional recognition algorithm, which is about 0.2dB. At the same time, when the signal-to-noise ratio is low, landform recognition can also achieve the preset recognition accuracy. Compared with two traditional recognition algorithms, the final recognition error results are shown in the fig 10.

(a) low geomorphological complexity

(b) moderate geomorphological complexity

(c) high geomorphological complexity

Fig.10 Recognition accuracy results of three algorithms under different geomorphic complexity

Three different landform recognition methods recognize three landforms with different complexity in the range of -10dB to 20dB SNR, and the recognition error is shown in Figure 10. As the complexity of landform increases gradually, the recognition error curve of the algorithm fluctuates. When the complexity of landform increases, the recognition error curves presented by different algorithms become more unstable, especially the traditional recognition algorithm 2. With the change of SNR, the angular measurement error oscillates sharply and appears extremely unstable. However, the measurement error of the recognition algorithm proposed in this paper is still at the low point of the error of the three angular measurement algorithms, which shows the superiority of the proposed algorithm.

IV. CONCLUSION

This paper proposes a landscape recognition algorithm for a polarized detector based on the optimal projection, which can be used for terrain recognition by a low-altitude flight radar platform. The characteristic parameters and projection basements composed of the characteristic values of the target scattering matrix are defined. By referring to the related Krogager's idea of decomposition of the target scattering matrix, the rotational invariant matrix of standard scattering bodies with parameters is established, and the polarization scattering matrix of terrains in the detection region is projected onto the standard basements so as to obtain optimal projection coordinates of the target scattering matrix onto every standard basement, and further determine the geomorphic properties. Finally, the feasibility and superiority of the proposed algorithm are experimentally validated. The obtained results show that terrains can be effectively distinguished.

REFERENCES

[1] X. S. Wang. "Status and prospects of radar polarimetry techniques," *Journal of Radar*, vol. 5, no. 2, pp. 119-136, 2016.

[2] D. H. Dai, B. Liao, S. P. Xiao, et al. "Advancements on radar polarization information acquisition and processing," *Journal of Radar*, vol. 5, no. 2, pp. 148-175, 2016.

[3] X. J. Song. "Radar target recognition based on polarization feature," *Radar Science and Technology*, vol. 14, no. 1, pp. 39-44, 2016.

[4] F. Y. Wang, D. Luo, H. W. Liu. "Radar target classification based on some invariant properties of the polarization," *Radar Science and Technology*, vol. 11, no. 2, pp. 165-172, 2013.

[5] X. H. Shao, A. Z. Li, F. B. Yan, et al. "Target recognition method based on weight by complex number," *Journal of Nanjing University of Science and Technology (Natural Science)*, vol. 33, no. 4, pp. 450-454, 2009.

[6] M. R. Beauchamp, V. Chandrasekar. "Dual polarization radar characteristics of wind turbines with ground clutter and precipitation," *IEEE Transaction on Geoscience and Remote Sensing*, vol. 54, no. 8, pp. 4833-4846, 2016.

[7] R. Xu, "Missile-borne embedded real-time radar signal processing system design and research," M.S. thesis, Xidian University. Xi'an, China, 2014.

[8] Y. Chen, H. C. Zhao, S. Chen, et al. "Imaging algorithm for missile-borne SAR using the fractional Fourier transform," *Acta Phys Sin*, vol. 63, no. 11, pp. 118403, 2014.

[9] L. Z. Song, X. L. Qiao, Q. Wu. "A kind of guidance radar with polarization diversity and its signal design for low probability of intercept," *Systems Engineering and Electronics*, vol. 31, no. 12, pp. 2853-2858, 2009.

[10] E. Krogager. "New decomposition of the radar target scattering matrix," *Electronics Letters*, vol. 26, no. 8, pp. 1525-1527, 1990.

[11] M. X. Gao, J. Yang, Y. N. Peng. "Extraction of target characteristics in polarimetric radar remote sensing," *Chinese Journal of Radio Science*, vol. 19, no. 4, pp. 418-422, 2004.

[12] N. N. Rao, X. B. Chen, J. B. Zhou, et al. "Research on ground clutter modeling of airborne cognitive radar based on digital elevation model data," *Journal of University of Electronic Science and Technology of China*, vol. 45, no. 4, pp. 511-519, 2016.

[13] H. Wang, T. H. Gao. "Training algorithm of adaptive neural fuzzy inference system based on improved SRUKF," *IAENG International Journal of Computer Science*, vol. 44, no. 4, pp. 396-403, 2017.

[14] D. Urynbassarova, B. Z. Li, Z. C. Zhang. "A convolution theorem for the polynomial Fourier transform," IAENG International Journal of Applied Mathematics, vol. 47, no. 4, pp. 381-387, 2017.